Albers *et al. Geothermal Energy* (2025) 13:23
https://doi.org/10.1186/s40517-025-00347-4

Geothermal Energy

RESEARCH Open Access

In-situ thermal properties of grouting materials in borehole heat exchangers

Anna Albers[1*], Petra Huttenloch[2], Yannick Reduth[3], Roman Zorn[2], Hagen Steger[1] and Philipp Blum[1]

*Correspondence:
anna.albers@kit.edu

[1] Karlsruhe Institute of Technology (KIT), Institute of Applied Geosciences (AGW), Kaiserstraße 12, 76131 Karlsruhe, Germany
[2] European Institute for Energy Research (EIFER), Emmy-Noether-Straße 11, 76131 Karlsruhe, Germany
[3] Steinbeis Research Institute for Solar and Sustainable Thermal Energy Systems (Solites), Meitnerstraße 8, 70563 Stuttgart, Germany

Abstract

The thermal properties of grouting materials characterise the heat transfer around borehole heat exchangers (BHE). However, these properties are typically determined in the laboratory. Thus, this study aims to assess the properties of grouting materials in the field. Two BHE grouted with two different grouting materials within unsaturated loess and limestone were excavated up to a depth of 15 m. Collected field samples show higher thermal conductivities by 13% ($W/S = 0.3$) and 35% ($W/S = 0.8$) than laboratory samples of the same material. These differences in thermal properties are mainly related to the filtration of the grouting suspension. In addition, with a short-time enhanced thermal response test (ETRT), 17% lower in-situ thermal conductivities are determined than in comparison with the field samples. The deviations are attributed to the geometry of the borehole, the trajectory of the BHE pipes and the heating cable. Thereby, this study shows the limitations when transferring laboratory-derived properties to a field site and emphasises the importance of considering site conditions, such as geology and hydrogeology.

Keywords: Backfill material, Enhanced thermal response test (ETRT), Field study, Filtration, Grout, Thermal conductivity, Volumetric heat capacity

Introduction

Ground source heat pump (GSHP) systems using borehole heat exchangers (BHE) present a sustainable technology to meet the heating and cooling demands of residential and office buildings (Bayer et al. 2012; Blum et al. 2010). The boreholes are often backfilled with grouting materials to stabilise the borehole and hinder vertical groundwater flow (IEA ECES 2020; Javadi et al. 2018) avoiding major damages (Fleuchaus and Blum 2017). In addition, the grouting materials must ensure efficient heat transfer from the subsurface to the BHE (Allan and Kavanaugh 1999). Thus, knowledge of the thermal properties of the grouting materials is crucial for an optimal design of GSHP systems.

The thermal response test (TRT) is a standard method to evaluate the thermal properties of the subsurface in situ (Spitler and Gehlin 2015). In a conventional TRT, a defined heat load is injected into or extracted from the ground by circulating the heat transfer fluid through the BHE pipes. The temperature response to the heat load is logged at the inlet and outlet of the BHE (Gehlin 2002; Raymond et al. 2011). An effective thermal conductivity λ_{eff} representing the entire BHE can be derived using analytical models

(e.g., Li and Lai 2015). Hence, several studies have used TRT to investigate the grout's thermal properties. By evaluating the thermal response time-dependently, the early time data can represent the grout thermal properties (Bozzoli et al. 2011; Li et al. 2019). However, the early response is also influenced by the fluid-to-pipe and pipe-to-grout heat transfer processes. The concept of equivalent diameter was introduced to simplify the complex geometry of the borehole into a single parameter and applied in analytical solutions to describe the early temperature response (e.g., Lamarche and Beauchamp 2007; Shirazi and Bernier 2013; Wei et al. 2016 and references therein). Nevertheless, conventional TRTs can only provide one effective thermal conductivity value, which represents the entire length of the BHE. One advancement of the conventional TRT is the enhanced thermal response test (ETRT), also described as enhanced geothermal response test (EGRT), where the defined heat load is applied by a heating cable and the temperature response is measured depth-specifically at a fibre optic cable (Wilke et al. 2020). This setup offers the advantage of early time data evaluation, since the cables are directly placed within the grout. Riegger et al. (2012) introduced the short-time ETRT for detecting grouting defects defined by a distinct difference in the thermal conductivity between the fluid-filled void and the grouting material. By defining characteristic periods of the heating and recovery phase of an ETRT, thermal conductivities can be attributed to the different materials of the BHE system. (1) In the first period of a few seconds (Riegger et al. 2012) to a few minutes (Zhang et al. 2020), the temperature increase can be attributed to the heating cable or hybrid cable itself. (2) In the second period of several minutes, the temperature increase is predominately influenced by the borehole including the BHE pipes and the grouting material. (3) In the third period, with increasing test time the evaluated thermal conductivities approach a stable value that can be attributed to the ground thermal conductivity. By plotting the temperature increase about the heating time in a semi-logarithmic plot, these three periods can be distinguished via break points showing material changes. Riegger et al. (2012) applied the short-time ETRT in a field experiment and demonstrated the principle with a numerical model. Moreover, Heidinger and Fabritius (2017) successfully applied the short-time ETRT at a different study site with a heating time of 1.5 h. Zhang et al. (2020) also conducted a short-time ETRT experiment at a BHE that was backfilled with medium-sized sand. They attributed the duration between 5 min and about 14 min heating time to the borehole properties. However, no information was given on the borehole diameter.

Aside from in-situ experiments, Javadi et al. (2022) investigated varying grouting materials in sandbox experiments. For these, they manufactured columns of different grouting materials by curing the materials in moulds of 1 m height. Then, they placed the cured materials in silica sand and conducted thermal tests, evaluating the influence of defects on the results. Furthermore, they developed a numerical model that was validated with the results from the sandbox experiments as the experiments were conducted under the defined conditions. However, therefore, the curing conditions did not represent conditions as they would occur in a sandy subsurface. In this regard, Colombero et al. (2016) and Bucci et al. (2018) conducted a field experiment by constructing a 7 m deep, grouted BHE in a quarry. The geology was characterised by gravel and sand. After 1.5 months, they excavated the grouted borehole and visually examined the grout integrity. They demonstrated defects and voids, especially at interfaces, where the geology

changed. However, the grouting materials were not analysed in terms of their material properties.

To summarise, with the short-time ETRT, a method was introduced that can be applied to evaluate the thermal conductivity of grouting materials in situ. However, validation of the method is difficult as more information is needed on the thermal properties of the grouting materials in the field. Commonly, the thermal properties of grouting materials are analysed at laboratory conditions from samples manufactured in the laboratory (Albers et al. 2024a). Commercially available grouting materials are specified with the properties determined in the laboratory. However, these properties can differ in the field. Several studies showed that curing grouting materials in a natural geology can include filtration processes (Domes 2015; Domes and Benz 2015; Eklund and Stille 2008; McKinley and Bolton 1999). Filtration describes the removal of water from the cement suspension, where the suspended particle size is smaller than the pore size of the natural filter (Domes 2015; McKinley and Bolton 1999). The particle concentration in the suspension increases, and a filter cake is formed. The filtration of cement suspensions is studied mainly in geotechnical engineering, e.g., regarding the grouting of anchors (Domes and Benz 2015) or tunnels (Eklund and Stille 2008). Moreover, Theophil et al. (2023) recently demonstrated that the same processes are relevant for the grouting of BHE.

Thus, the objective of this study is to examine the in-situ thermal properties of grouting materials in BHEs. Grouted BHEs with two different grouting materials are, therefore, constructed in a large-scale field experiment. After conducting field experiments, the boreholes are excavated up to a depth of 15 m. Field samples of the grouting materials are collected, and their thermal properties are characterised by extensive laboratory experiments. The results are compared with grouting samples manufactured in the laboratory and discussed about filtration. Moreover, they are used for comparison with in-situ thermal conductivities determined with the short-time ETRT at one BHE. This study, therefore, provides new insights into the properties of grouting materials in the field from a unique study site. Our findings improve the reliability of material specifications and support the interpretation of field experiments.

Materials and methods

Study site

The study site is situated in Merdingen, southwest Germany (Fig. 1a). The geology is characterised by loess in the upper 14.5 m (Fig. 1b, Table 1). Below, weathered limestone is encountered, followed by solid limestone from about 21 m below ground level (bgl). The entire borehole is within the vadose zone. Eight boreholes are drilled on the edge of a quarry using a down-the-hole hammer, from which two boreholes (B1 and B2) are discussed within this study (Fig. 1b).

The geometry and specifications of the boreholes are summarised in Table 1. Double U-pipe BHEs are installed in the boreholes (Table 1). Borehole B1 is equipped with a hybrid cable, containing fibre optic and heating cables (HELUKOM A-DSQ(ZN)B2Y; 1×4 G 50/125 + Cu 4×0.5 mm^2; total cable length = 69.8 m), on the outside of one of the U-pipes. The grouting materials are mixed on the construction site with a colloidal mixer (GERTEC, IS-33-E) and filled into the borehole (Table 1).

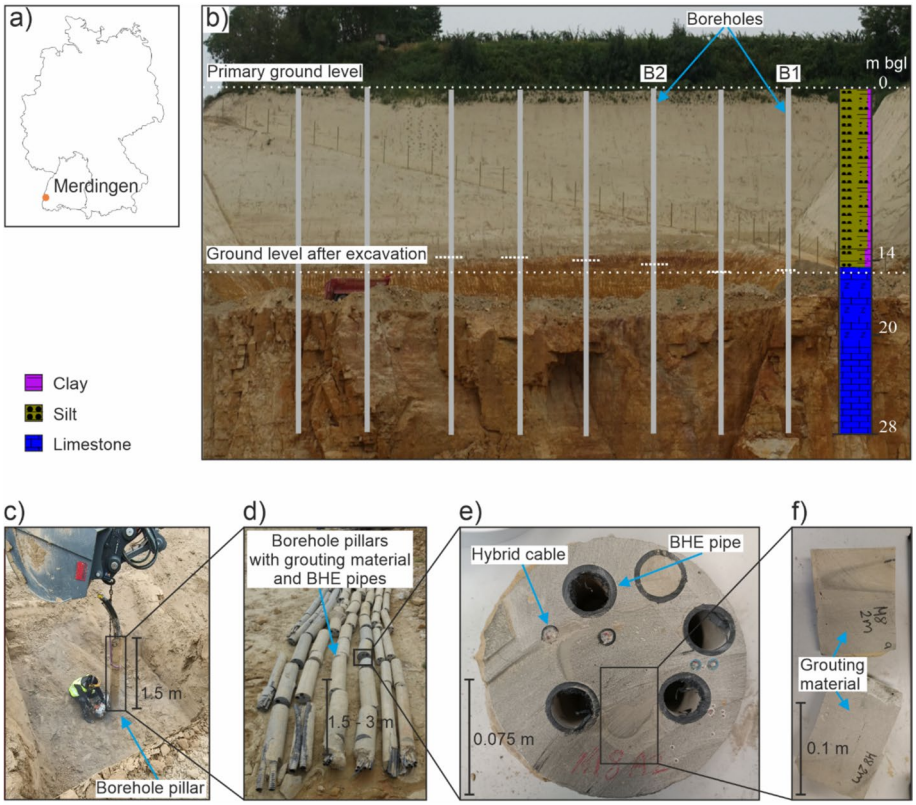

Fig. 1 **a** Location of the field site, **b** geology, the position of the boreholes B1 and B2 before the deconstruction and the study site after the excavation, **c**–**f** sampling and sample preparation for the laboratory analyses

Table 1 Borehole geometry, specifications of the BHE and grouting materials

Borehole	**B1**	**B2**
Borehole depth (m)	28	26
Base of loess (m)	14.5	13
Base of weathering zone (m)	23	18.3
Borehole diameter	150/132	219/190
Borehole casing (m)	19.5	4
Borehole heat exchanger (BHE)		
Type	Double U-pipe, PE100 RC	
Manufacturer	STÜWA Konrad Stükerjürgen GmbH	
Outer radius r_{po} (m)	0.016	
Inner radius r_{pi} (m)	0.013	
Thermal conductivity λ_p (W m^{-1} K^{-1})	0.42	
Grouting material	**M1**	**M2**
Manufacturer	Schwenk Zement KG	Hans G. Hauri KG
Material	Füllbinder EWMplus	Zeotherm2.0
Batch	13.05.2022	2022-KW45
Water–solid ratio	0.3	0.8
Thermal conductivity λ (W m^{-1} K^{-1})*	> 2.0	2.0
Suspension density ρ_{sus} (g cm^{-3})*	1.94	1.48

* Manufacturer value

Sampling

During the construction of the BHEs, material from the grouting suspension is sampled on-site and cured in the laboratory as *batch* sample ("Sample preparation"). About 10–11 months after the construction, the boreholes are deconstructed with an excavator up to a depth of about 15 m (Fig. 1b, c). During excavation, the grouted boreholes, including the BHE pipes and the installed measurement technique, are sampled in pillars with lengths between 1.5 and 3 m (Fig. 1c, d). At least every 2 m along these pillars, grouting samples are taken (Fig. 1e). These *field* samples are further cut to prepare them for laboratory analyses (Fig. 1e, "Laboratory analyses"). Moreover, eight core samples are taken from the soil surrounding B1 at several depths (1.5, 4.0, 5.2, 6.0, 8.0, 11.0, 13.2 and 14.5 m).

Laboratory analyses

Sample preparation

A *laboratory* sample of the grouting material is manufactured based on the procedure recommended by Albers et al. (2024a). The grouting material is mixed in the laboratory with a dissolver (IKA Eurostar 60 digital, dissolver stirrer R1300, diameter = 80 mm) at a mixing speed of 2000 rpm for 5 min. The laboratory samples and the batch samples are cured in the laboratory for 28 days. For this purpose, the suspension is filled in moulds with a defined geometry (Albers et al. 2024a). The moulds are stored under deionised water at room conditions (20 ± 2 °C).

An overview of the different samples and methods is presented in Table 2. For the sake of clarity, the methods are referred to with the assigned names during the entire manuscript.

Material properties

The material properties are determined in accordance with the German Industrial Standards (DIN). Water content w (–) is determined by oven drying at 105 °C according to DIN EN ISO 17892-1 (Deutsche Norm 2022b). Wet bulk density ρ_b (g cm^{-3}) is determined using immersion weighing according to DIN EN ISO 17892-2 (Deutsche Norm 2015). From dried and ground samples, solid density ρ_s (g cm^{-3}) is measured with the pycnometer method according to DIN ISO 17892-3 (Deutsche Norm 2016). Dry bulk density ρ_d (g cm^{-3}), porosity ϕ (–) and saturation S_r (–) are calculated (Prinz and Strauß 2018).

Table 2 Samples and methods applied in this study to determine the thermal conductivity (λ_g) and specific heat capacity ($c_{p,g}$) of the grouting materials

Sample	Material	Manufacturing	Curing	Analyses	Thermal properties
Laboratory	M1, M2	In the laboratory	laboratory for 28 days	TPS[1], DSC[2]	λ_g, $c_{p,g}$
Batch	M1, M2	In the field using a colloidal mixer			
Field	M1, M2		in-situ for 11 months		
In-situ	M1		in-situ for 1–3 months	ETRT	λ_g

[1] Transient Plane Source (TPS) method; [2]Differential Scanning Calorimetry (DSC)

Particle size analysis is conducted with a laser particle analyser (PSA 1190 L/D, *Anton-Paar*, accuracy ± 3%) in accordance with DIN ISO 13320 (Deutsche Norm 2022a). The grain size of the samples is < 250 mm. Before the measurement, soil samples are mixed with 0.2% sodium pyrophosphate solution; grout samples are measured in ethanol. The samples are dispersed with ultrasound (50 W) for 1 min. For soil samples, ultrasound is used during the 1-min measurement. Grout samples are measured without ultrasonic at defined mixing (350 rpm) and pumping speed (300 rpm). The data is analysed using Kalliope software (*Anton-Paar*) according to the Fraunhofer model.

The pore size distribution is determined using a mercury porosimeter (Autopore III Analyzer, *Micromeritics Instruments Corporation*) in accordance with DIN ISO 15901-1 (Deutsche Norm 2019). For this purpose, the samples are cut into cubes with an edge length of approximately 5 mm. The materials are oven-dried at 105 °C.

Thermal conductivity is measured with the transient plane source method (Hot-Disk TPS1500, *C3 Prozess- und Analysentechnik*, Germany; measurement uncertainty ± 2%). The samples are measured at room temperature (20 ± 2 °C) in a closed, thermally insulated container that is protected from sunlight. At least four repeated measurements are conducted. The specific heat capacity of the grouting materials is measured with a differential scanning calorimeter (DSC, No. 204 F1 Phönix, *Netzsch*, Germany) applying the sapphire comparison method according to DIN EN ISO 11357-4 (Deutsche Norm 2021) and described in Albers et al. (2024a) in detail. DSC measurements are conducted on ground, dry samples (oven-dried at 105 °C). The specific heat capacity at original water content $c_{p,f}$ (kJ kg^{-1} K^{-1}) is the weighted arithmetic mean of the specific heat capacities of the components. Volumetric heat capacity $\rho c_{p,f}$ (MJ m^{-3} K^{-1}) is calculated with the bulk density.

In-situ experiments

Enhanced thermal response tests (ETRT)

A short-time ETRT is conducted about 1 month after the construction of the BHEs at B1, when the undisturbed subsurface temperature has been reached again. An average specific heat load of 22.1 W m^{-1} is applied for 13 h using a DC-power supply (Power Ten Inc., R86 D-200100; 200V/100A). Current and voltage are logged during the entire heating time (Table 3). The temperature is measured at 240 s intervals using distributed temperature sensing (DTS) with a measurement interval of 1 m (Table 3, dual-ended measurement).

Table 3 Technical specifications of the measurement instruments used for voltage, current and temperature measurement

Parameter	Instrument	Uncertainty
Voltage	ALMEMO 2890-9, *Ahlborn*	± 0.1% of the full-scale value of 200 V + 2 digits + 0.03% of the measurement value + 2 digits
Current	ALMEMO 2890-9, *Ahlborn*	± 0.1% of the full-scale value of 200 V + 2 digits + 0.03% of the measurement value + 2 digits + 0.5% uncertainty of the shunt
Temperature	N4386B, *Agilent*, *AP Sensing*	± 0.2 K

Evaluation

The short time ETRT is evaluated for depth-specific thermal conductivities of the grouting material (λ_g) and of the subsurface (λ_{eff}) by applying the Infinite Line Source (ILS) model (Carslaw and Jaeger 1959) with a parameter estimation approach:

$$T(r,t) - T_0 = \frac{q}{4\pi\lambda_{\text{eff}}} E_i\left[\frac{r^2}{4\alpha t}\right] + qR_{\text{th}} \tag{1}$$

with $T(r,t)$ being the temperature at a defined distance r from the heat source and a specific time t, T_0 being the undisturbed subsurface temperature at time $t=0$, q being the specific heat load calculated depth-specifically according to Albers et al. (2024b), E_i being the potential integral, r being the radius of the hybrid cable ($r_{\text{cable}}=0.006$ m) and α being the thermal diffusivity calculated as

$$\alpha = \frac{\lambda_{\text{eff}}}{\rho c_p} \tag{2}$$

The volumetric heat capacities are assumed to be $\rho c_{p,g}=2.71$ MJ m^{-3} K^{-1} for the grouting material and $\rho c_{p,s}=1.92$ MJ m^{-3} K^{-1} for the subsurface. As the hybrid cable is installed in a loop parallel to the BHE pipes, both shanks of the cable are evaluated separately, resulting in two values for each depth interval.

The temperature data is evaluated for different evaluation times. The later temperature increase is expected to be mainly influenced by the thermal conductivity of the subsurface (Riegger et al. 2012). To derive grout thermal conductivities, only the early time data is characteristic. Using the equation for the penetration depth of the heat signal:

$$r = \sqrt{\frac{4}{e^{\gamma}}\alpha t} \tag{3}$$

The theoretical time when the heat signal reaches the borehole wall is calculated. The heating cables are assumed to be positioned in the centre of the borehole. The distance r is set to $r=r_b-r_{\text{cable}}$. The calculated time is then used as a criterion until when the temperature increase can be attributed to the borehole.

Results and discussion

Laboratory and batch samples

The influence of the manufacturing process on the material properties is investigated by comparing the material properties of the grouting samples manufactured in the laboratory (laboratory sample) and on-site (batch sample). Differences are observed in the water content (Table 4). Material M1 has a 17% lower water content comparing the batch to the laboratory sample, whereas M2 has a 6% higher water content. However, the other properties show no significant differences (Table 4). This indicates that the dissolver used in the laboratory ensures a sufficient mixing of the components. Hence, the mixing procedure in the laboratory is comparable to that in the field. Differences between laboratory and field samples ("Grouting materials") are, therefore, not attributed to the mixing procedure. However, it is to be expected that inhomogeneities and

Table 4 Material properties of the laboratory, batch and field samples of the grouting materials M1 and M2

Material	**M1**		
Sample	**Laboratory**	**Batch**	**Field** **Mean of *n* = 9 [min; max]**
Water content w (%)	27.7 ± 0.2	23.1 ± 0.3	12.6 [11.6 ± 1.0; 14.1 ± 1.9]
Bulk density ρ_b (g cm^{-3})	1.96 ± 0.02	2.03 ± 0.02	2.19 [2.13 ± 0.06; 2.22 ± 0.02]
Porosity φ (%)	42.2 ± 1.7	38.6 ± 1.8	27.5 [25.7 ± 1.9; 30.0 ± 3.2]
Saturation S_r (%)	101 ± 6	99 ± 7	89 [85 ± 16; 93 ± 12]
Thermal conductivity λ_g (W m^{-1} K^{-1})	1.98 ± 0.06	1.99 ± 0.06	2.3 [1.85 ± 0.05; 2.45 ± 0.05]
Volumetric heat capacity $\rho c_{p,g}$ (MJ m^{-3} K^{-1})	3.02 ± 0.07	2.92 ± 0.07	2.61 [2.50 ± 0.10; 2.74 ± 0.16]
Material	**M2**		
Sample	**Laboratory**	**Batch**	**Field** **Mean of *n* = 6 [min; max]**
Water content w (%)	71.1 ± 0.1	75.5 ± 0.3	35.6 [31.8 ± 0.5; 42.5[a]]
Bulk density ρ_b (g cm^{-3})	1.57 ± 0.02	1.55 ± 0.02	1.82 [1.73 ± 0.06; 1.87 ± 0.02]
Porosity φ (%)	65.2 ± 1.7	66.7 ± 1.6	48.8 [46.5 ± 1.7; 53.5 ± 2.9]
Saturation S_r (%)	100 ± 4	100 ± 4	98 [97 ± 8;100 ± 9]
Thermal conductivity λ_g (W m^{-1} K^{-1})	1.72 ± 0.04	1.68 ± 0.08	2.29 [2.19 ± 0.06; 2.40 ± 0.05]
Volumetric heat capacity $\rho c_{p,g}$ (MJ m^{-3} K^{-1})	3.48 ± 0.06	3.58 ± 0.07	3.16 [3.09 ± 0.09; 3.22 ± 0.14]

[a] Single measurement

inconsistencies occur more easily when mixing on-site with a colloidal mixer. Thus, the quality of the grouting material may vary between different mixed batches.

Field samples

Grouting materials

Depth-specific results of the field samples are shown for the upper 15 m bgl in Fig. 2. The comparison of laboratory and field samples shows significant changes in the properties of the grouting materials.

The thermal conductivities of material M1 range between 1.85 ± 0.05 and 2.45 ± 0.05 W m^{-1} K^{-1} (Fig. 2a). The average thermal conductivity is 2.26 W m^{-1} K^{-1}. The thermal conductivities of M2 range between 2.19 ± 0.06 and 2.40 ± 0.05 W m^{-1} K^{-1}. The average thermal conductivity is 2.29 W m^{-1} K^{-1}. The average thermal conductivity significantly increased for both grouting materials compared to the laboratory sample. For M1, an increase of 13% is observed; for M2, an increase of 35% is detected. These higher thermal conductivities represent improved thermal properties in the field regarding the heat transfer between the subsurface and the BHE pipe. The average volumetric heat capacities vary between 2.50 ± 0.10 and 2.74 ± 0.16 MJ m^{-3} K^{-1} for M1, and between 3.09 ± 0.09 and 3.22 ± 0.14 MJ m^{-3} K^{-1} for M2 (Fig. 2b). Hence, consequently lower values are measured in the field than for the laboratory sample.

The differences in the material properties can explain the differences in the thermal properties. Volumetric heat capacity is a combined parameter of the specific heat capacity of dry samples, the water content and the bulk density ("Material properties"). The water content of the field samples is 55% lower for M1 and 50% for M2 (Fig. 2c). Laboratory samples are manufactured so that complete saturation of the samples is obtained. In

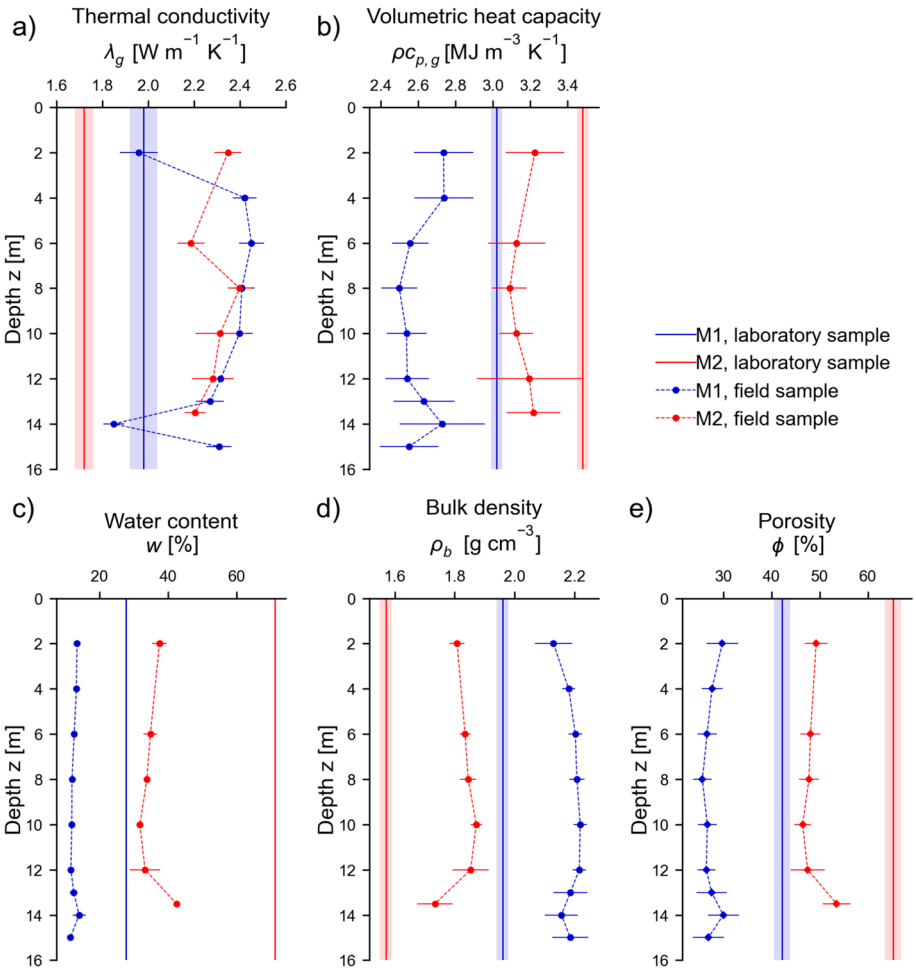

Fig. 2 Material properties **a** thermal conductivity λ_g, **b** volumetric heat capacity ρc_p, **c** water content w, **d** bulk density ρ_b and **e** porosity φ of the grouting materials M1 and M2 from field samples compared to the laboratory samples

contrast, the saturation of the field samples is reduced. Material M1 shows saturation of only 85–93%. The reduction is not that significant for M2, with saturation of 97–100%. Furthermore, the field samples have a higher bulk density than the laboratory samples, with 2.19 g cm^{-3} instead of 1.96 g cm^{-3} for M1, and 1.82 g cm^{-3} instead of 1.57 g cm^{-3} for M2 (Fig. 2d). The lower water contents of the field samples have a higher impact on the volumetric heat capacity than the higher bulk density.

Higher thermal conductivities of grouting materials are related to lower porosities, since the solid matrix of the sample usually has a higher thermal conductivity than the pore fluid (Allan 1997), which can include both water and/or air. The porosity of all field samples is significantly reduced compared to the laboratory samples (Fig. 2e). A clear correlation, however, cannot be established within the values. Nevertheless, for material M1, the two field samples with the highest porosities (at depth $z=2$ m and 14 m) have the lowest thermal conductivities (Fig. 2a, e).

Not only the porosity but also the average pore throat diameters of the field samples are lower than those of the laboratory samples (Fig. 3).

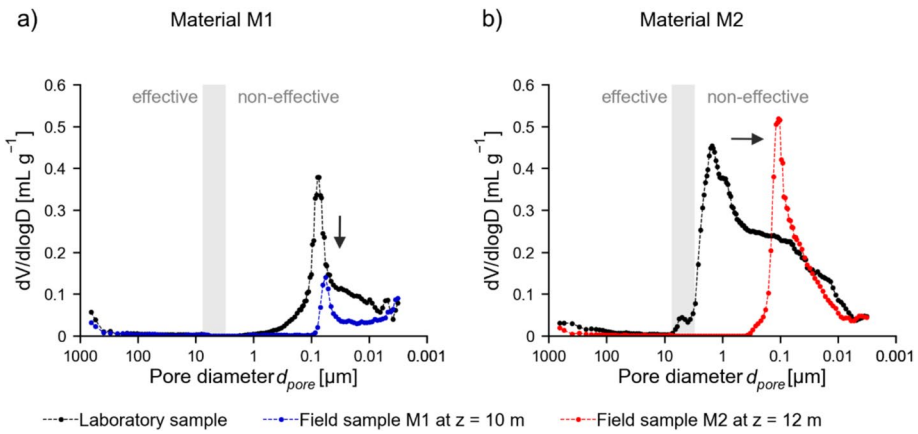

Fig. 3 Pore size distribution from mercury intrusion porosimetry of the two grouting materials **a** M1 and **b** M2, highlighting the differences between the laboratory samples and the field samples at two specific depths *z*. The value ranges of hydraulically effective and non-effective pore diameters are indicated

Material M1 has an average pore diameter of 0.017 µm (field sample) instead of 0.021 µm (laboratory). M2 has an average pore diameter of 0.024 µm (field sample) instead of 0.055 µm (laboratory). Especially for material M2, the laboratory sample shows a peak at a diameter of about 1.5 µm, which shifts towards 0.1 µm for the field sample (Fig. 3b). M1 also shows a shift towards lower pore diameters. Here, a bimodal pore size distribution evolves within the field sample. Thus, the decrease in the pore volume can mainly be attributed to the reduction of the bigger pores. However, all samples show pore sizes below the hydraulically effective pore diameter (Busch and Luckner 1973). Thus, the grouting materials are appropriate materials to hinder fluid flow.

In summary, the higher bulk densities, the reduction of the pore space and the decrease of the water content indicate agglomeration of the solid material within the field samples. The differences between laboratory and field samples are more profound for material M2 than for M1. Some sample-specific observations limit the interpretations of the material properties. A closer look at the sample at 2 m bgl (M1) reveals a material change within the sample (Fig. 1f), which could indicate a flow channel. This demonstrates that the grouting material within the borehole does not necessarily represents one homogeneous material. However, due to the necessary sample size for thermal conductivity analysis, no separate analysis of the two different materials could be conducted.

Soil properties

The differences in the material properties between laboratory and field samples can be explained by the difference in the backfilling process and the hydration conditions. In the laboratory, the samples are cured in moulds stored under water, ensuring controlled conditions and complete saturation. In contrast, in the field, the samples are in direct contact with the natural subsurface. Thus, the properties of the subsurface have significant influence on the results of the grouting and its achieved properties. Several studies show that filtration processes can influence the curing of grouting materials in a natural geology (Domes 2015; Domes and Benz 2015; Eklund and Stille 2008; McKinley and

Bolton 1999). Hence, the properties of the subsurface as a filter medium for the grouting suspension are described.

Table 5 summarises the properties determined for the subsurface.

In this study, grouting is only conducted in the vadose zone. The upper meters (ground level to 11 m bgl) are unsaturated loess with water contents of about 10% and saturations between 24 and 36%. Bulk densities are determined at about 1.5 g cm^{-3}. Below 11 m bgl, water contents increase up to 65%. The base of the excavated zone is defined by a strongly weathered limestone (Fig. 1b). A core sample of the weathered material and a grouting sample at the same depth is ensured to be collected. However, further excavation below this zone is not possible due to the increasing strength of the subsurface. Thus, the investigation within this study focuses on the accessible 15 m of the study site (Fig. 1b). The particle size distribution presented in Fig. 4 illustrates the loess material as a well-sorted silt. The raw materials of M1 and M2 can be defined as widely distributed silt, with a bigger particle size for M2. The filter criterion by Terzaghi can be applied (Terzaghi et al. 1996):

$$N = \frac{D_{15}}{d_{85}} \tag{4}$$

with D_{15} being the 15% particle diameter of the filter (soil) and d_{85} being the 85% particle diameter of the filtrate (grouting material). Values of $N = 0.4$ (M1) and $N = 0.1$ (M2) are calculated, which characterise the loess as an efficient filter for the two grouting materials ($N < 4$, Terzaghi et al. 1996).

Water can be transported within the soil through Darcy or capillary flow. Darcy flow can be defined through hydraulic conductivity. The hydraulic conductivity of the loess (at 8 m bgl) is evaluated to 3×10^{-7} to 1×10^{-6} m s^{-1} ($\pm 4.8\%$, $T = 10$ °C) and, therefore, can be relevant for flow transport processes. The ability for capillary flow can be estimated through pore size distribution. The average pore diameter is evaluated between 0.28 and 0.84 µm, corresponding to a capillary height of 8.9 to 27.0 m. The weathered limestone has a significantly higher average pore diameter of 42.2 µm, corresponding only to a capillary height of 0.2 m.

Besides the soil properties, the pressure difference and the properties of the grouting suspension also have to be considered for the filtration process. The pressure difference between the borehole and the surrounding ground is defined by the pressure

Table 5 Material properties of the soil samples

Material (depth and number of samples *n*)	**Loess (1.5 to 13.2 m)**	**Weathered limestone (14.5 m)**
	Mean of *n* = 7; [min; max] [a]	***n* = 1 [a]**
Water content w (%)	11.6 [7.9; 18.7]	13.7
Bulk density ρ_b (g cm^{-3})	1.56 [1.46 ± 0.06; 1.77 ± 0.02]	2.01 ± 0.11
Porosity φ (%)	47.9 [44.8; 51.0]	36.5
Saturation S_r (%)	34 [24; 62]	67
Thermal conductivity λ_g (W m^{-1} K^{-1})	1.09 [0.91 ± 0.03; 1.39 ± 0.08]	1.07 ± 0.06
Volumetric heat capacity $\rho c_{p,g}$ (MJ m^{-3} K^{-1})	1.83 [1.68; 2.10]	2.02

[a] single measurements without measurement uncertainty

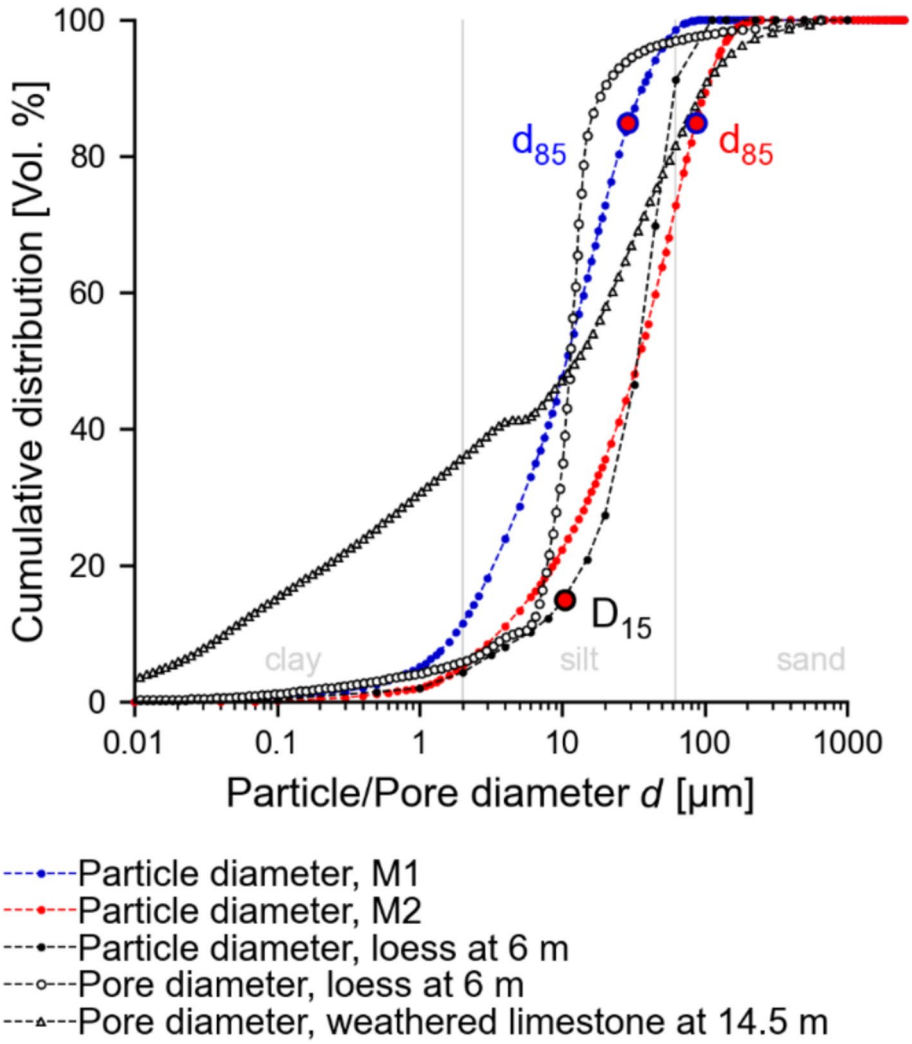

Fig. 4 Pore size distribution of the loess (depth $z = 6$ m) and the weathered limestone ($z = 14.5$ m), and particle size distribution of the loess and the grouting materials (raw material before hydration) with the significant particle diameters d_{85} and D_{15} for applying the filter criterion by Terzaghi et al. (1996), demonstrating that the soil effectively filters the grouting particles

of the suspension column, which also depends on the density of the grouting material. Thus, higher depths experience a higher pressure, which could result in stronger filtration in these areas. The suspension density of the grouting materials is measured to 1.96 g cm^{-3} at 29.5 °C (M1) and 1.53 g cm^{-3} at 31.2 °C (M2). Both materials are designed to provide good work and flow ability for the grouting of boreholes. This can be demonstrated with Marsh funnel flow times (1 L) of 47 s (M1) and 45 s (M2). Furthermore, the W/S, together with the composition of the sample (i.e., clay content, cement content, water absorption capacity), influences the degree of filtration. M2 has a significantly higher W/S of 0.8 than M1 with a W/S of 0.3. The results presented in the previous chapter "Grouting materials" highlight that M2 shows a higher water reduction than M1 (Fig. 2c).

Overall, the subsurface properties support the explanation of filtration processes, resulting in the variation of the material properties. We expect the conditions of this study site to represent an extreme scenario with grouting in the vadose zone without groundwater. However, filtration processes can also occur below the groundwater table as long as the pressure in the suspension exceeds the groundwater pressure (e.g., Schlötzer 1995) and the filter criterion by Terzaghi et al. (1996) is fulfilled.

In-situ test

Enhanced thermal response test (ETRT)

In-situ thermal conductivities are determined with an ETRT. Depth-specific evaluation is shown in Fig. 5 for three distinct evaluation times. Surface effects, such as diurnal temperature changes and steep temperature gradients along the length of the fibre optic cable, can affect the results. Thus, the upper meter of the BHE is excluded from analysis and only depths ≥ 2 m bgl are presented. The in-situ results are compared to the results of the field samples for the grouting material and soil.

In Fig. 5, from left to right, increasing evaluation times are considered. Figure 5a shows the evaluation of the first 5–50 min of heating time. Under the theoretical consideration that the temperature increase at the beginning of the ETRT is mainly influenced by the grouting material within the borehole, grout thermal conductivities are most likely assessed during this period. An average thermal conductivity of 1.9 W m^{-1} K^{-1} is evaluated and, thus, is lower than that of the field samples. At most depths, the in-situ thermal conductivities scatter slightly around 2.0 W m^{-1} K^{-1}. However, significantly lower thermal conductivities <1 W m^{-1} K^{-1} are evaluated at 14 m bgl. The thermal conductivities are separately presented for the two shanks of the hybrid cable. At some depths,

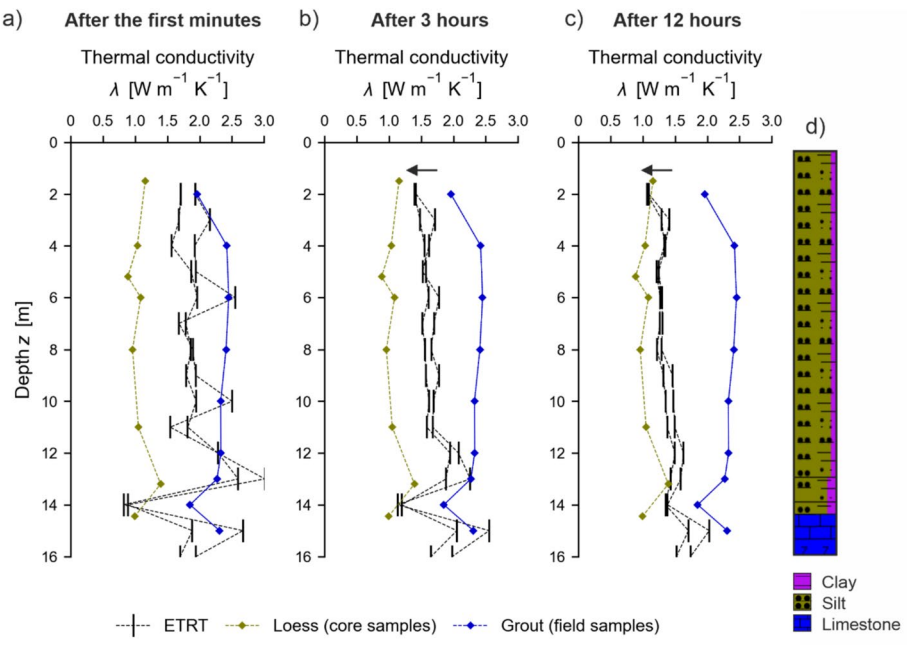

Fig. 5 Depth-specific thermal conductivities evaluated for **a** the time when the heat signal is expected to reach the borehole wall, **b** 3 h, **c** 12 h, compared to laboratory-derived thermal conductivities of field samples and **d** to the borehole profile

thermal conductivities vary significantly between the two shanks, which indicates a higher uncertainty of the results. Especially at 11 and 13 m bgl, the difference between the two values is high, with 29% and 34%.

Figure 5b shows the evaluation after 3 h of heating when the temperature increase is expected to be a mixed signal of the borehole and the subsurface. Since the grouting material has a higher thermal conductivity than the surrounding loess, the thermal conductivities decrease with increasing evaluation time (Fig. 5a, b). The average thermal conductivity is calculated to be 1.7 W m^{-1} K^{-1}. The results already reflect the lower in-situ thermal conductivities of the soil at about 5 m bgl and the higher value at about 13 m, which are measured from the core samples.

Figure 5c presents the evaluation after 12 h of heating when the temperature increase should be predominately influenced by the subsurface material. An average thermal conductivity of 1.4 W m^{-1} K^{-1} is evaluated, which is still higher than the thermal conductivity of the core samples.

To illustrate the evolution of the temperature increase with time, the temperature increase is plotted against the natural logarithm of the heating time in Fig. 6. The temperature data is stacked for the depths 2 to 12 m bgl, as according to the results from Figs. 2 and 5c, a homogeneous loess layer can be distinguished. Moreover, by stacking the data, the uncertainty of the temperature measurement is reduced.

By plotting the results on a logarithmic scale, the temperature increase shows significant break points in the data, which can indicate a change of material with different thermal conductivity (Riegger et al. 2012; Zhang et al. 2020). The different phases of heating the BHE system can easily be distinguished. The temperature shows a strong

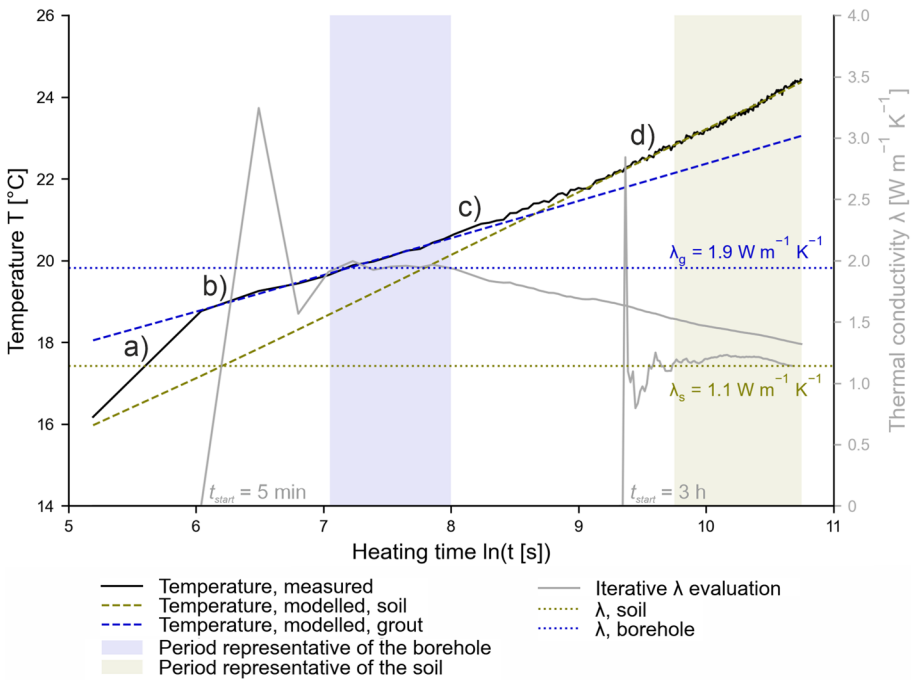

Fig. 6 Evaluation of the short-time ETRT for stacked data (2–12 m bgl), illustrating the different phases of the temperature increase due to **a** the heating cable, **b** the borehole, **c** increasing influence of the soil, **d** soil-dominated

first increase due to the heating of the hybrid cable material (Fig. 6a). Then, a weaker increase due to the high thermal conductivity of the borehole is observed (Fig. 6b). A transition zone with increasing influence of the thermal properties of the loess can be distinguished, which is indicated by a progressively stronger increase in temperature (Fig. 6c). At later heating times, the temperature increase is stronger than at the beginning of the test and is predominately influenced by soil properties (Fig. 6d).

In addition, the iterative thermal conductivity evaluation (Fig. 6 in grey) is illustrated for a starting time of 5 min and a starting time of 3 h. The blue-shaded area highlights the time period of the ETRT for which a stable thermal conductivity of about 1.9 W m^{-1} K^{-1} can be evaluated, which is representative for the borehole. Afterwards, a gradual decrease of the thermal conductivity can be observed, which is related to a stronger increase in temperature and, thus, an increasing influence of the soil on the temperature response (Phase c). This part of the iterative curve is not suitable to derive a representative thermal conductivity value as it does not converge to a stable value. The iterative evaluation also highlights the importance of the starting time when evaluating an ETRT, as a stable thermal conductivity value for the subsoil cannot be established within the 12 h of the test when selecting an early starting time. The olive-shaded area represents a stable thermal conductivity of about 1.1 to 1.2 W m^{-1} K^{-1} that is obtained with a starting time of 3 h, thereby reducing the influence of the borehole. The late-time evaluation (3–12 h) is in excellent agreement with the laboratory measurements. The thermal conductivity of the loess is evaluated to 1.1 W m^{-1} K^{-1} (laboratory 1.09 W m^{-1} K^{-1}). This value aligns with standard ranges provided by the VDI 4640, part 1. A thermal conductivity range between 0.4 and 1.0 W m^{-1} K^{-1} is given for dry material, and between 1.1 and 3.1 W m^{-1} K^{-1} for water-saturated material (Verein Deutscher Ingenieure 2010). With water saturations about 34%, the evaluated loess thermal conductivity is reasonable. The thermal conductivity of the borehole is evaluated to 1.9 W m^{-1} K^{-1}. Hence, it is lower than the thermal conductivity of the field samples.

Discussion

Several challenges in analysing the in-situ thermal conductivities of the grouting material can explain the discrepancy between the results of the different measurement methods. Figure 7 highlights the challenges attributed to the borehole itself.

The borehole consists of the grouting material, the water-filled BHE pipes, and the measurement equipment, such as hybrid cables and cables for temperature and pressure sensors. By illustrating the positions of the BHE pipes and the hybrid cables at depths of 2 to 15 m, Fig. 7 also demonstrates that the geometry within the borehole is not symmetric at all. The position of the pipes changes significantly within 1 to 2 m. Prediction of the trajectory of the pipes is hardly possible. Moreover, the borehole represents a system with holes and contact failures, which can be observed in Fig. 7 at depths 13 and 14 m bgl. In comparison, the thermal conductivities of field samples are measured from material samples without defects or cracks, and ensuring a good contact surface. Thus, the comparison between in-situ measurement and field samples is expected to contain these uncertainties, as the measured temperature signal represents a mixed signal of the entire borehole system. This can explain lower in-situ thermal conductivities evaluated for the grouting material.

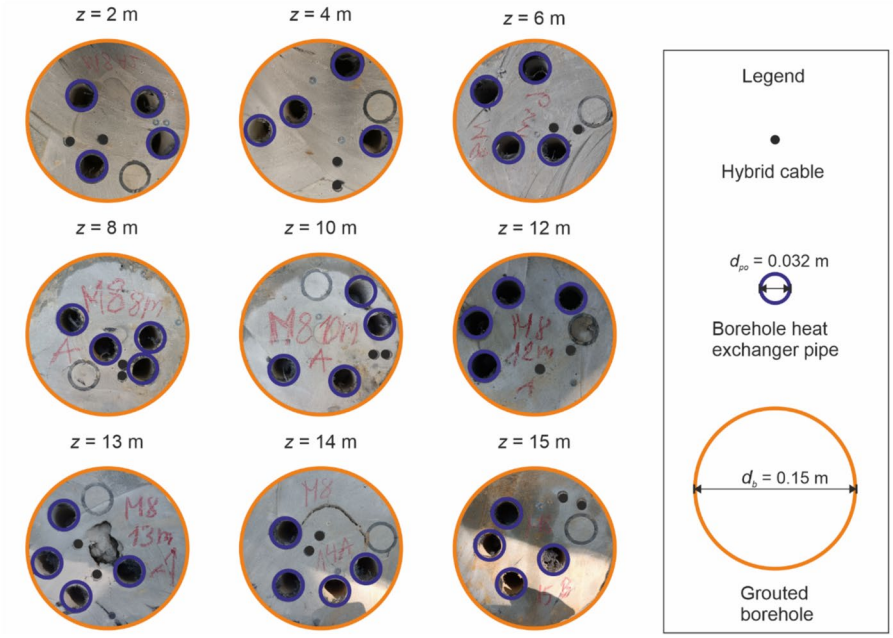

Fig. 7 Position of the BHE pipes and the hybrid cables within borehole B1 for specific depths *z* collected from the grouted borehole pillar (Fig. 1e)

Furthermore, several assumptions are made when evaluating the short-time ETRT. As shown in Fig. 7, the position of the hybrid cable is not in the centre of the borehole but changes with depth. The distance of the hybrid cable from the borehole centre varies between 12 and 64 mm. The distance between the two shanks of the hybrid cable varies between 11 and 35 mm. When the hybrid cable is close to the borehole wall, the temperature signal quickly becomes a mixed response signal of the grout and the soil. When the distance between the hybrid cables itself is high, the difference in the evaluated values of both shanks can become high. Moreover, the specific heat load during the first minutes of the test can be inaccurate, as the heat signal of the two hybrid cables in one depth overlaps only after a few minutes. If the distance between the hybrid cables itself is high, the specific heat load can be overestimated. This issue was also shown by Riegger et al. (2012). They highlighted a successive overlay of the two heat loads of both shanks of the cable after the initial heating period of the cable. They concluded that the position of the hybrid cable has a relevant influence on the evaluation of the thermal conductivity of the grouting material and can result in an error of 13–14%.

In addition, when evaluating the early time data of the ETRT, only a limited number of data points are analysed, which again increases the uncertainty of the estimate. Stacking data of several depth intervals can reduce this uncertainty. The borehole profile shows a homogenous layer of loess (Fig. 1b). By averaging the temperature data along the corresponding length interval of the hybrid cable, the grout and soil thermal conductivities can be determined more reliably, as demonstrated in Fig. 6. Furthermore, the time interval of the DTS measurement can be reduced to generate a higher number of data points. However, as a smaller time interval increases the uncertainty of the DTS measurement, a balance must be found.

In summary, the short-time ETRT has proven effective for in-situ estimation of the thermal conductivity of the borehole. The direct contact between the heating cable and the grouting material is a significant benefit of the ETRT as it allows for the evaluation of the early temperature response. Observed differences between field samples and in-situ measurements are primarily attributed to the distinct analytical approaches for material versus borehole system.

Conclusion

This study examines the in-situ properties of grouting materials. By comparing laboratory grout samples manufactured in the laboratory at defined conditions, field samples collected during the excavation of grouted BHEs, and in-situ measurements, the following conclusions can be made:

1. The field samples of two different grouting materials show higher thermal conductivities by 13% ($W/S=0.3$) and 35% ($W/S=0.8$) than laboratory samples of the same material.
2. This increase can be explained by filtration in the natural soil during the curing process of the grouting materials.
3. Comparison of grout thermal conductivities between the field samples and the in-situ measurement shows 17% lower values for the results from the in-situ measurement. In-situ thermal conductivities are evaluated to an average of 1.9 $\mathrm{W\ m^{-1}\ K^{-1}}$, whereas for field samples, an average of 2.3 $\mathrm{W\ m^{-1}\ K^{-1}}$ is measured. Uncertainties about the short-time ETRT are attributed to the geometry of the borehole, the trajectory of the BHE pipes and the position of the hybrid cable.

The findings of this study provide further insights into the properties of grouting materials on site, which contribute to the reliability of the simulation and design of GSHP systems. Thermal conductivities from laboratory samples help compare materials under controlled conditions, but they serve only as initial reference values, as field properties may vary. Developing grouting materials should ideally also consider the interactions between grout and subsurface. However, the findings are limited to the evaluated study site, where filtration is the dominant process. The interactions between the grout and the subsurface are complex, material-specific, site-specific and not easily generalised. Hence, further research should investigate the properties of grouting materials at different geological and hydrogeological conditions, where other processes, such as penetration and groundwater flow, are also considered.

Applying the short-time ETRT, the thermal conductivity of the borehole system is evaluated rather than the thermal conductivity of the grouting material. The findings suggest that the iterative evaluation procedure can reliably provide thermal conductivity values for the borehole and the subsurface. Stacking of the temperature data of homogeneous lithological zones is recommended to reduce the uncertainty of the temperature signal and of the arbitrary cable position.

Abbreviations

BHE	Borehole heat exchanger
bgl	Below ground level

c_p Specific heat capacity [kJ kg^{-1} K^{-1}]
$c_{p,f}$ Specific heat capacity at original water content [kJ kg^{-1} K^{-1}]
$c_{p,g}$ Specific heat capacity of the grouting material [kJ kg^{-1} K^{-1}]
$c_{p,s}$ Specific heat capacity of the subsurface [kJ kg^{-1} K^{-1}]
d_b Borehole diameter [m]
D_{15} Particle diameter of the loess with 15% smaller particles [µm]
d_{85} Particle diameter of the grouting material with 85% smaller particles [µm]
DIN Deutsches Institut für Normung (German Institute for Standardisation)
d_{po} Outer pipe diameter [m]
d_{pore} Pore diameter [µm]
DSC Differential scanning calorimetry
DTS Distributed temperature sensing
EGRT Enhanced geothermal response test
E_i Exponential integral
ETRT Enhanced thermal response test
GSHP Ground source heat pump
ILS Infinite line source
k Hydraulic conductivity [m s^{-1}]
N Filter criterion by Terzaghi [–]
PE Polyethylene
q Specific heat load [W m^{-1}]
r Radial distance from heat source [m]
r_b Borehole radius [m]
r_{cable} Radius of the hybrid cable [m]
r_{pi} Inner pipe radius [m]
r_{po} Outer pipe radius [m]
R_{th} Thermal resistance [K m W^{-1}]
S_r Saturation [%]
t Time [s]
T Temperature [°C]
T_0 Undisturbed subsurface temperature [°C]
TRT Thermal response test
w Water content [%]
W/S Water–solid ratio
z Depth [m]
α Thermal diffusivity [m^2 s^{-1}]
γ Euler's constant
λ Thermal conductivity [W m^{-1} K^{-1}]
λ_{eff} Effective thermal conductivity [W m^{-1} K^{-1}]
λ_g Grout thermal conductivity [W m^{-1} K^{-1}]
λ_p Pipe thermal conductivity [W m^{-1} K^{-1}]
λ_s Soil thermal conductivity [W m^{-1} K^{-1}]
φ Porosity [%]
ρ_b Bulk density [g cm^{-3}]
ρ_{sus} Suspension density [g cm^{-3}]
ρc_p Volumetric heat capacity [MJ m^{-3} K^{-1}]
$\rho c_{p,f}$ Volumetric heat capacity at original water content [MJ m^{-3} K^{-1}]
$\rho c_{p,g}$ Volumetric heat capacity of the grout [MJ m^{-3} K^{-1}]
$\rho c_{p,s}$ Volumetric heat capacity of the soil [MJ m^{-3} K^{-1}

Acknowledgements
The authors would like to thank the company Hans G. Hauri KG Mineralstoffwerke for providing the test site at the edge of their quarry and for their support in the deconstruction process. The provision of the grouting materials by Hans G. Hauri KG Mineralstoffwerke and Schwenk Zement KG is gratefully acknowledged. The authors would also like to thank Tom Brand from Solites for his support during the field deconstruction process; Madeline Dantin and Lucas Homann for their help with the laboratory experiments, as well as Dr. Ruth Haas Nüesch and Stephan Gehlsen for providing the particle size analysis data. The helpful comments of the two reviewers are also gratefully acknowledged.

Author contributions
A.A., P.H., H.S. and R.Z. developed the methodology and study design. A.A., P.H. and H.S. conducted the laboratory analyses. A.A. and R.Z. evaluated the data. Y.R., A.A. and H.S. deconstructed the BHE. A.A., R.Z. and H.S. conducted the field experiments. H.S. and R.Z. acquired the funding. H.S. and R.Z. and Y.R. handled the project administration. P.B. provided supervision. A.A. created the figures and prepared the first draft. All authors reviewed and approved the final manuscript.

Funding
Open Access funding enabled and organized by Projekt DEAL. This study was carried out within the framework of the joint project QEWSplus, which is funded by the Federal Ministry for Economic Affairs and Climate Action, Germany (FKZ: 03EE4020D, E, H).

Availability of data and materials
The datasets used and/or analysed during the current study are available from the corresponding author upon reasonable request.

Declarations

Ethics approval and consent to participate
Not applicable.

Competing interests
The authors declare no competing interests.

Received: 25 November 2024 Accepted: 23 April 2025
Published online: 14 May 2025

References

Albers A, Huttenloch P, Zorn R, Steger H, Blum P. Determination of thermal properties of grouting materials for borehole heat exchangers (BHE). Geotherm Energy. 2024a;12(1):36.
Albers A, Steger H, Zorn R, Blum P. Evaluating an enhanced thermal response test (ETRT) with high groundwater flow. Geotherm Energy. 2024b;12(1):1.
Allan M. Thermal conductivity of cementitious grouts for geothermal heat pumps, FY Progress Report. BNL 65129. New York: Brookhaven National Laboratory; 1997.
Allan M, Kavanaugh S. Thermal conductivity of cementitious grouts and impact on heat exchanger length design for ground source heat pumps. HVAC&R Res. 1999;5(2):85–96.
Bayer P, Saner D, Bolay S, Rybach L, Blum P. Greenhouse gas emission savings of ground source heat pump systems in Europe: a review. Renew Sustain Energy Rev. 2012;16(2):1256–67.
Blum P, Campillo G, Münch W, Kölbel T. CO2 savings of ground source heat pump systems—a regional analysis. Renew Energy. 2010;35(1):122–7.
Bozzoli F, Pagliarini G, Rainieri S, Schiavi L. Estimation of soil and grout thermal properties through a TSPEP (two-step parameter estimation procedure) applied to TRT (thermal response test) data. Energy. 2011;36(2):839–46.
Bucci A, Prevot AB, Buoso S, De Luca DA, Lasagna M, Malandrino M, et al. Impacts of borehole heat exchangers (BHEs) on groundwater quality: the role of heat-carrier fluid and borehole grouting. Environ Earth Sci. 2018;77(5):175.
Busch KF, Luckner L. Geohydraulik. 2. Leipzig: Deutscher Verlag für Grundstoffindustrie; 1973.
Carslaw HS, Jaeger JC. Conduction of Heat in Solids. 2nd ed. Oxford: Oxford Science Publications; 1959.
Colombero C, Comina C, Guiliani A, Mandrone G. Ultrasonic equipment aimed to detect grouting homogeneity in geothermal heat exchangers; 2016
Deutsche Norm. DIN EN ISO 17892-2 Geotechnical investigation and testing—Laboratory testing of soil—Part 2: determination of bulk density (ISO 17892-2:2014); German version EN ISO 17892-2:2014. Beuth Verlag GmbH; 2015.
Deutsche Norm. DIN ISO 17892-3, Geotechnical investigation and testing—laboratory testing of soil—part 3: Determination of particle density (ISO 17892-3:2015, Corrected version 2015-12-15); German version EN ISO 17892*3:2015. Beuth Verlag GmbH; 2016.
Deutsche Norm. DIN ISO 15901-1, Evaluation of pore size distribution and porosity of solid materials by mercury porosimetry and gas adsorption—part 1: mercury porosimetry (ISO 15901-1:2016). Beuth Verlag GmbH; 2019.
Deutsche Norm. DIN EN ISO 11357-4, Plastics—differential scanning calorimetry (DSC)—part 4: determination of specific heat capacity (ISO 11357-4:2021); German version EN ISO 11357-4:2021. Beuth Verlag GmbH; 2021.
Deutsche Norm. DIN ISO 13320:2022-12, Particle size analysis—Laser diffraction methods (ISO 13320:2020). Beuth Verlag GmbH; 2022a. https://www.beuth.de/de/-/-/358912542. Accessed 8 July 2024.
Deutsche Norm. DIN EN ISO 17892-1, Geotechnical investigation and testing—Laboratory testing of soil—part 1: determination of water content (ISO 17892-1:2014 + Amd 1:2022); German version EN ISO 17892-1:2014 + A1:2022. Beuth Verlag GmbH; 2022b.
Domes X. Cement grouting during installation of ground anchors in non-cohesive soils [Dissertation]. [Trondheim]: Norwegian University of Science and Technology Faculty of Engineering Science and Technology Department of Civil and Transport Engineering; 2015.
Domes X, Benz T. Untersuchungen zur Zementfiltration während der Herstellung von Verpressankern in nichtbindigen Böden. Bautechnik. 2015;92(9):605–16.
Eklund D, Stille H. Penetrability due to filtration tendency of cement-based grouts. Tunn Undergr Space Technol. 2008;23(4):389–98.
Fleuchaus P, Blum P. Damage event analysis of vertical ground source heat pump systems in Germany. Geotherm Energy. 2017;5(1):1–15.
Gehlin S. Thermal response test: Method Development and evaluation [Dissertation]. [Luleå]: Luleå University of Technology; 2002.
Heidinger P, Fabritius A. Faseroptische Temperaturmessungen - zur Detektierung der Hinterfüllungsqualität: Schlussbericht mit UpDate zu Drittmessungen in Deutschland. Karlsruhe: Swiss Federal Office of Energy SFOE; 2017 Apr. Report No.: E1712-01P. https://www.bfe.admin.ch/bfe/de/home/news-und-medien/publikationen.exturl.html/aHR0cHM6Ly9wdWJkYi5iZmUuYWRtaW4uY2gvZGUvc3VjaGU_cG/FnZT0yNjQmeD0x.html
IEA ECES. Quality management in design, construction and operation of borehole systems. IEA Technology Collaboration Programme on Energy Conservation through Energy Storage (IEA ECES); 2020. https://iea-es.org/wp-content/uploads/public/IEA-ECES-ANNEX-27-Final-Report-20201118.pdf
Javadi H, Mousavi Ajarostaghi S, Rosen M, Pourfallah M. A comprehensive review of backfill materials and their effects on ground heat exchanger performance. Sustainability. 2018;10(12):4486.

Javadi H, Urchueguía JF, Badenes B, Mateo MÁ, Nejad Ghafar A, Chaudhari OA, et al. Laboratory and numerical study on innovative grouting materials applicable to borehole heat exchangers (BHE) and borehole thermal energy storage (BTES) systems. Renew Energy. 2022;194:788–804.
Lamarche L, Beauchamp B. New solutions for the short-time analysis of geothermal vertical boreholes. Int J Heat Mass Transf. 2007;50(7–8):1408–19.
Li M, Lai ACK. Review of analytical models for heat transfer by vertical ground heat exchangers (GHEs): a perspective of time and space scales. Appl Energy. 2015;151:178–91.
Li M, Zhang L, Liu G. Estimation of thermal properties of soil and backfilling material from thermal response tests (TRTs) for exploiting shallow geothermal energy: sensitivity, identifiability, and uncertainty. Renew Energy. 2019;132:1263–70.
McKinley JD, Bolton MD. A geotechnical description of fresh cement grout—filtration and consolidation behaviour. Mag Concr Res. 1999;51(5):295–307.
Prinz H, Strauß R. Ingenieurgeologie. Berlin: Springer, Berlin Heidelberg; 2018.
Raymond J, Therrien R, Gosselin L, Lefebvre R. A review of thermal response test analysis using pumping test concepts. Ground Water. 2011;49(6):932–45.
Riegger M, Heidinger P, Lorinser B, Stober I. Auswerteverfahren zur Kontrolle der Verfüllqualität in Erdwärmesonden mit faseroptischen Temperaturmessungen. Grundwasser. 2012;17(2):91–103.
Schlötzer C. Filtrationsverhalten von Dichtsuspensionen an flüssigkeitsgestützten Erdwänden [Dissertation]. [Hannover]: Universität Hannover; 1995.
Shirazi AS, Bernier M. Thermal capacity effects in borehole ground heat exchangers. Energy Build. 2013;67:352–64.
Spitler JD, Gehlin SEA. Thermal response testing for ground source heat pump systems—an historical review. Renew Sustain Energy Rev. 2015;50:1125–37.
Terzaghi K, Peck RB, Mesri G. Soil mechanics—a new chapter in engineering science, vol. 3. New York: Wiley; 1996.
Theophil T, Reduth Y, Mangold D. Interaktion von ErdwärmesondenVerfüllbaustoffen mit dem Untergrund. bbr Sonderheft; 2023.
Verein Deutscher Ingenieure. VDI 4640, part 1: thermal use of the underground, fundamentals, approvals, environmental aspects; 2010.
Wei J, Wang L, Jia L, Zhu K, Diao N. A new analytical model for short-time response of vertical ground heat exchangers using equivalent diameter method. Energy Build. 2016;119:13–9.
Wilke S, Menberg K, Steger H, Blum P. Advanced thermal response tests: a review. Renew Sustain Energy Rev. 2020;119:109575.
Zhang B, Gu K, Shi B, Liu C, Bayer P, Wei G, et al. Actively heated fiber optics based thermal response test: a field demonstration. Renew Sustain Energy Rev. 2020;134: 110336.

Publisher's Note